A MODEL FOR AXIAL MAGNETIC BEARINGS INCLUDING EDDY CURRENTS

Ladislav Kučera
International Center for Magnetic Bearings, ETH Zurich
Switzerland

Markus Ahrens
International Center for Magnetic Bearings, ETH Zurich
Switzerland

ABSTRACT

This paper presents an analytical method of modelling eddy currents inside axial bearings. The problem is solved by dividing an axial bearing into elementary geometric forms, solving the Maxwell equations for these simplified geometries, defining boundary conditions and combining the geometries. The final result is an analytical solution for the flux, from which the impedance and the force of an axial bearing can be derived. Several impedance measurements have shown that the analytical solution can fit the measured data with a precision of approximately 5%.

INTRODUCTION

Modelling magnetic bearings is necessary to achieve reasonable results for magnetic force and bearing losses in order to design bearings and amplifiers. Furthermore, controller design is based on a model of the plant including magnetic bearings. Magnetic bearings are usually modelled as equivalent electrical circuits. With simple models neglecting eddy currents, hysteresis, saturation and material nonlinearities, it is possible to achieve approximations for the magnetic force which are sufficient for most applications. Nevertheless, better modelling can improve bearing design and system behaviour. For some applications such as self sensing bearings a more precise model is necessary.
The absolute permeability μ describes the relationship between the magnetic flux density B and the magnetic field strength H (see equation (5)). The relative permeability μ_r is material dependent, the permeability of vacuum μ_0 is constant. For simple models μ_r can be assumed to be constant, but for real materials μ_r depends on the magnetic field strength (i.e. $\mu_r = \mu_r(H)$). With increasing magnetic field strength the gradient μ decreases (to a limit value μ_0). Therefore, the magnetic flux density is nearly constant for high field strengths (*saturation*). While increasing and decreasing H, the flux density B has different values for forward or backward loops due to *hysteresis* of the material. There are complex mathematical models such as the Preisach model [May91] to describe hysteresis, but these do not have an analytical solution.
Changing magnetic fields inside conducting materials cause currents to flow. These *eddy currents* have a large influence on the behaviour of magnetic bearings. The main goal of this paper

is to achieve an analytical description of a bearing model including eddy currents. Nonlinear material behaviour is considered in numerical calculations. Hysteresis is neglected in this paper. For elementary geometric forms, analytical solutions for eddy currents can be found. These solutions are sufficient to describe the behaviour of axial bearings. The elementary geometric forms are a semi-infinite plate, a rotationally symmetric plate and a semi-infinite cylinder.

ELEMENTARY GEOMETRIC FORMS

Electromagnetic fields and, therefore, eddy currents also can be described using Maxwell's equations ([Küp90], [Jac83]). In order to achieve analytical solutions it is necessary to divide an axial bearing into elementary geometric forms. Contrary to numerical results,analytical solutions can be more useful for bearing and controller design. Finite Element analysis can solve two or three-dimensional problems and more complex geometric forms. These numerical calculations are therefore used to verify analytical results and simplifications.

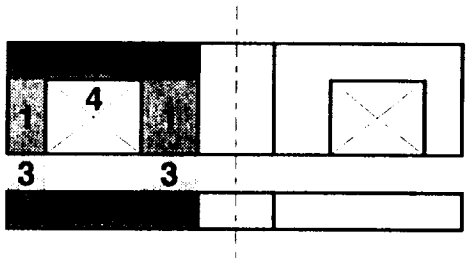

(1) Semi-infinite cylinder
(2) Rotational symmetric plate
(3) Air gap
(4) Coil with N turns

Figure 1: Cross section of an axial bearing. The bearing is divided into elementary forms.

Maxwell's Equations

Considering that the frequencies of the currents and fields are sufficiently low so that we can neglect the displacement current $\partial \boldsymbol{D}/\partial t$, Maxwell's equations can be written as

$$\mathrm{curl}\boldsymbol{E} = -\frac{\partial \boldsymbol{B}}{\partial t} = -\frac{\mathrm{d}\boldsymbol{B}}{\mathrm{d}\boldsymbol{H}}\frac{\partial \boldsymbol{H}}{\partial t} \tag{1}$$

$$\mathrm{curl}\boldsymbol{H} = \boldsymbol{J} \tag{2}$$

$$\mathrm{div}\boldsymbol{B} = 0 \tag{3}$$

Here $\boldsymbol{E}$ is the electric field strength and $\boldsymbol{J}$ the current density. The generalized Ohm's law, with the electric conductivity σ is given by:

$$\boldsymbol{J} = \sigma \boldsymbol{E} \tag{4}$$

The material equation is:

$$\boldsymbol{B} = \mu_0 \mu_r \boldsymbol{H} = \mu \boldsymbol{H} \tag{5}$$

Combining equations (1), (2), (4) and (5) we obtain:

$$\mathrm{curl}(\mathrm{curl}\boldsymbol{H}) = -\mu\sigma\frac{\partial \boldsymbol{H}}{\partial t} \tag{6}$$

A sinusoidal variation of the fields enables the transformation of equation (6) into the Fourier space. $\partial/\partial t$ can be replaced by $j\omega$ giving:

$$\mathrm{curl}(\mathrm{curl}\boldsymbol{H}) = -j\omega\mu\sigma\boldsymbol{H} = -\alpha^2\boldsymbol{H} \tag{7}$$

where:

$$\alpha = \sqrt{j\omega\mu\sigma} = (1+j)\sqrt{\frac{\omega\mu\sigma}{2}} \tag{8}$$

Maxwell's equations (2) and (3) can be integrated using the theorems of Stokes and Gauss (Θ: magnetomotive force , Φ: magnetic flux) to give:

$$\Theta = \int_{\partial A} \boldsymbol{H}\mathrm{d}\boldsymbol{s} = \sum \boldsymbol{I} + \int_{A} \boldsymbol{J}\mathrm{d}\boldsymbol{A} \tag{9}$$

$$\Phi = \int_{\partial V} \boldsymbol{B}\mathrm{d}\boldsymbol{A} \tag{10}$$

In the following sections, solutions for the elementary geometric forms *semi-infinite plate*, *rotational symmetric plate* and *semi-infinite cylinder* are given.

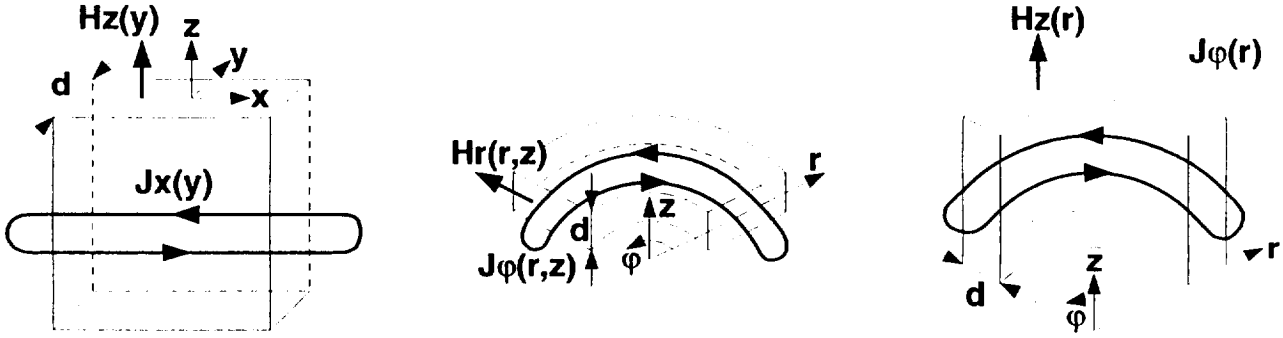

Figure 2: Cross section of
(a) a semi-infinite plate, (b) a rotational plate, (c) a semi-infinite cylinder

Semi-infinite Plate

A very long plate with thickness d and a magnetic field only in the z-direction has an eddy current flow in the x-direction. Equation (7) leads to the following differential equation:

$$\mathrm{curl}\begin{pmatrix} 0 \\ 0 \\ H_z \end{pmatrix} = \begin{pmatrix} \frac{\partial H_z}{\partial y} \\ 0 \\ 0 \end{pmatrix} = \begin{pmatrix} J_x \\ 0 \\ 0 \end{pmatrix} \tag{11}$$

$$\operatorname{curl}\begin{pmatrix} \frac{\partial H_z}{\partial y} \\ 0 \\ 0 \end{pmatrix} = \begin{pmatrix} 0 \\ 0 \\ -\frac{\partial^2 H_z}{\partial y^2} \end{pmatrix} = \begin{pmatrix} 0 \\ 0 \\ -\alpha^2 H_z \end{pmatrix} \tag{12}$$

$$\frac{\partial^2 H_z}{\partial y^2} = \alpha^2 H_z \tag{13}$$

with the general solution:

$$H_z(y) = c_1 e^{\alpha y} + c_2 e^{-\alpha y} \tag{14}$$

$$J_x(y) = \frac{\partial H_z}{\partial y} = c_1 \alpha e^{\alpha y} - c_2 \alpha e^{-\alpha y} \tag{15}$$

Rotational Symmetric Plate

$$\operatorname{curl}\begin{pmatrix} H_r \\ 0 \\ 0 \end{pmatrix} = \begin{pmatrix} 0 \\ \frac{\partial H_r}{\partial z} \\ 0 \end{pmatrix} = \begin{pmatrix} 0 \\ J_\varphi \\ 0 \end{pmatrix} \tag{16}$$

$$\operatorname{curl}\begin{pmatrix} 0 \\ \frac{\partial H_r}{\partial z} \\ 0 \end{pmatrix} = \begin{pmatrix} -\frac{\partial^2 H_r}{\partial z^2} \\ 0 \\ \frac{1}{r}\frac{\partial}{\partial r}\left(r\frac{\partial H_r}{\partial z}\right) \end{pmatrix} = \begin{pmatrix} -\alpha^2 H_r \\ 0 \\ 0 \end{pmatrix} \tag{17}$$

Equation (17) represents the following two differential equations:

$$\frac{\partial^2 H_r}{\partial z^2} = \alpha^2 H_r \tag{18}$$

$$\frac{1}{r}\frac{\partial H_r}{\partial z} + \frac{\partial^2 H_r}{\partial z \partial r} = 0 \tag{19}$$

The solution for the differential equations (18) and (19) can be found by separation of the variables:

$$H_r(r, z) = \mathcal{R}(r)\mathcal{Z}(z) \tag{20}$$

Equation (18) can be transformed to:

$$\frac{\partial^2 \mathcal{Z}}{\partial z^2} = \alpha^2 \mathcal{Z} \tag{21}$$

with the general solution:

$$\mathcal{Z}(z) = z_1 e^{\alpha z} + z_2 e^{-\alpha z} \tag{22}$$

Equation (19) can be transformed to:

$$\frac{1}{r}\mathcal{R} + \frac{\partial \mathcal{R}}{\partial r} = 0 \tag{23}$$

with the general solution:

$$\mathcal{R}(r) = r_1 \frac{1}{r} \tag{24}$$

Equation (22) and (24) lead to:

$$H_r(r,z) = \frac{1}{r}(c_1 e^{\alpha z} + c_2 e^{-\alpha z}) \tag{25}$$

Without regard for r, equation (25) is similar to equation (14) (the case of the semi-infinite plate).

Semi-infinite Cylinder

$$\text{curl} \begin{pmatrix} 0 \\ 0 \\ H_z \end{pmatrix} = \begin{pmatrix} 0 \\ -\frac{\partial H_z}{\partial r} \\ 0 \end{pmatrix} = \begin{pmatrix} 0 \\ J_\varphi \\ 0 \end{pmatrix} \tag{26}$$

$$\text{curl} \begin{pmatrix} 0 \\ -\frac{\partial H_z}{\partial r} \\ 0 \end{pmatrix} = \begin{pmatrix} 0 \\ 0 \\ -\frac{1}{r}\frac{\partial}{\partial r}\left(r\frac{\partial H_z}{\partial r}\right) \end{pmatrix} = \begin{pmatrix} 0 \\ 0 \\ -\alpha^2 H_z \end{pmatrix} \tag{27}$$

$$\frac{\partial^2 H_z}{\partial r^2} + \frac{1}{r}\frac{\partial H_z}{\partial r} - \alpha^2 H_z = 0 \tag{28}$$

The substitution $\bar{r} = \alpha r$ transforms the differential equation (28) into Bessel's equation:

$$\bar{r}^2 \frac{\partial^2 H_z}{\partial \bar{r}^2} + \bar{r}\frac{\partial H_z}{\partial \bar{r}} - \bar{r}^2 H_z = 0 \tag{29}$$

with the general solution:

$$H_z(\bar{r}) = c_1 I_0(\bar{r}) + c_2 K_0(\bar{r}) \tag{30}$$

or written without substitution:

$$H_z(r) = c_1 I_0(\alpha r) + c_2 K_0(\alpha r) \tag{31}$$

Here, I_0 is the modified Bessel function of first type and zeroth order and K_0 is the modified Bessel function of second type and zeroth order. More detailed information can be found in [AS65]. For calculations with Bessel functions, especially with complex arguments, a power series expansion is necessary. A solution without Bessel functions is therefore desirable.
It can be clearly seen that equation (31) leads to equation (14) when $R_i \gg d$ (R_i: inner radius of the cylinder). A numerical comparison of the results for equation (31) and equation (14) shows that the difference between these two equations is only significant for unrealistically small values of R_i ($R_i < d$).

An analysis of the cases of the semi-infinite cylinder and the rotational symmetric plate shows that these cases can be described with the equations of the semi-infinite plate. The problem of eddy currents in a semi-infinite plate is well known in the literature ([Sto74], [Küp90]), because the choice of lamination thickness is important for high power transformers and electrical machines.

BOUNDARY CONDITIONS

Solutions of differential equations require definitions of boundary conditions. Current field lines have to be closed. This is valid for eddy currents too. It is therefore assumed that eddy currents in a semi-infinite plate turn back at infinity. Eddy currents flow in one direction at one edge and in the other direction at the second edge (see figure 3 (a)). This solution is given in the literature ([Sto74], [Küp90]).
For a semi-infinite cylinder a second solution is possible. Contrary to a plate, a cylinder is geometrically closed and therefore eddy currents can flow in one direction (see figure 3 (b)). Calculations with the Finite Element program FEMAG ([Ins94]) produce this solution by default.

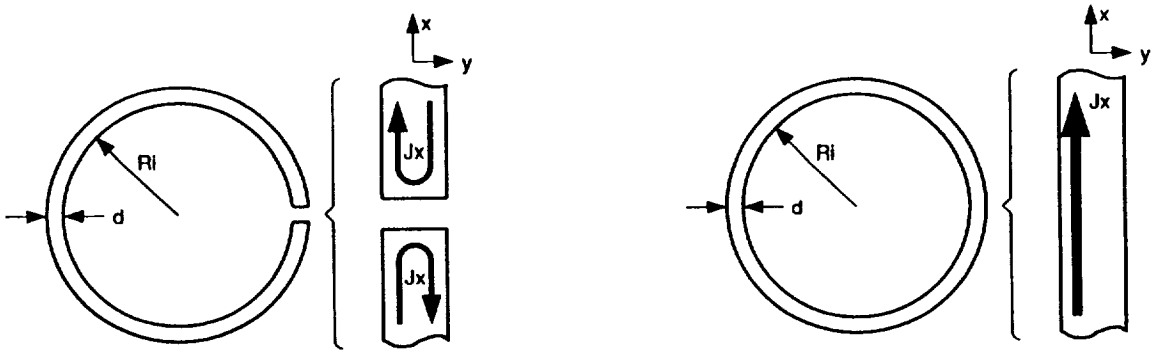

Case (a): A cylinder with an intersection. Eddy currents flow in two directions.

Case (b): A cylinder without an intersection. Eddy currents flow in one direction.

Figure 3: The two different boundary conditions. Cylinders with or without intersection.

Cylinder with intersection

The constants c_1 and c_2 of equations (14) and (15) can be found by defining two boundary conditions. The first boundary condition is given by

$$H_z(-\frac{d}{2}) = H_0 \tag{32}$$

The second boundary condition can be derived using Kirchhoff's law. The sum of all the currents has to be 0.

$$\int_{-\frac{d}{2}}^{\frac{d}{2}} J_x(y)\mathrm{d}y = 0 \tag{33}$$

Equation (33) can be written as:

$$H_z(\frac{d}{2}) = H_z(-\frac{d}{2}) \tag{34}$$

The solutions for H_z, J_x and the flux Φ with the boundary condition of a cylinder with intersection are as follows (A is the area of the cross section of a cylinder):

$$H_z(y) = H_0 \frac{\cosh(\alpha y)}{\cosh(\alpha \frac{d}{2})} \tag{35}$$

$$J_x(y) = \alpha H_0 \frac{\sinh(\alpha y)}{\cosh(\alpha \frac{d}{2})} \tag{36}$$

$$\Phi = \int_{-\frac{d}{2}}^{\frac{d}{2}} B \mathrm{d}A = \mu \frac{A}{d} \int_{-\frac{d}{2}}^{\frac{d}{2}} H_z(y) \mathrm{d}y = A \mu H_0 \frac{\tanh(\alpha \frac{d}{2})}{\alpha \frac{d}{2}} \tag{37}$$

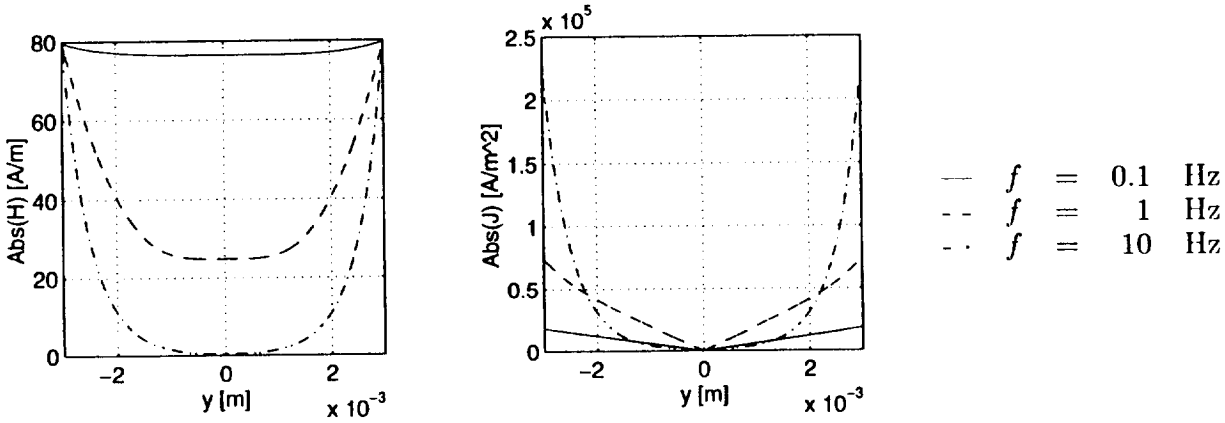

Figure 4: $|H_z(y)|$ and $|J_x(y)|$ for a cylinder with intersection.

Figure 4 shows the decrease of the H-field in the middle of the core and the increase of eddy currents near the surface of the core with increasing frequency. The following model parameters have been used.

d	=	$6 \cdot 10^{-3}$	m
A	=	$1.39 \cdot 10^{-3}$	m^2
μ_0	=	$4\pi \cdot 10^{-7}$	H/m
μ_r	=	5000	
H_0	=	79.6	A/m
B_0	=	$\mu_0 \mu_r H_0 = 0.5$	T
σ	=	$2 \cdot 10^7$	$(\Omega \mathrm{m})^{-1}$

Cylinder without intersection

In the case of a cylinder without intersection the start and end of the plate are fixed together and therefore eddy currents can have closed field lines and flow in one direction (the opposite

direction of the coil current).[1] The eddy current density at the outer surface of the core is zero.

c_1 and c_2 in equations (14) and (15) can be found by defining two boundary conditions. The first boundary condition is given by:

$$H_z(-\frac{d}{2}) = H_0 \tag{38}$$

The second boundary condition is given by:

$$J_x(\frac{d}{2}) = 0 \tag{39}$$

The solutions for H_z, J_x and Φ with the boundary condition of a cylinder without intersection are

$$H_z(y) = H_0 \frac{\cosh(\alpha\frac{d}{2} - \alpha y)}{\cosh(\alpha d)} \tag{40}$$

$$J_x(y) = \alpha H_0 \frac{\sinh(\alpha\frac{d}{2} - \alpha y)}{\cosh(\alpha d)} \tag{41}$$

$$\Phi = A\mu H_0 \frac{\tanh(\alpha d)}{\alpha d} \tag{42}$$

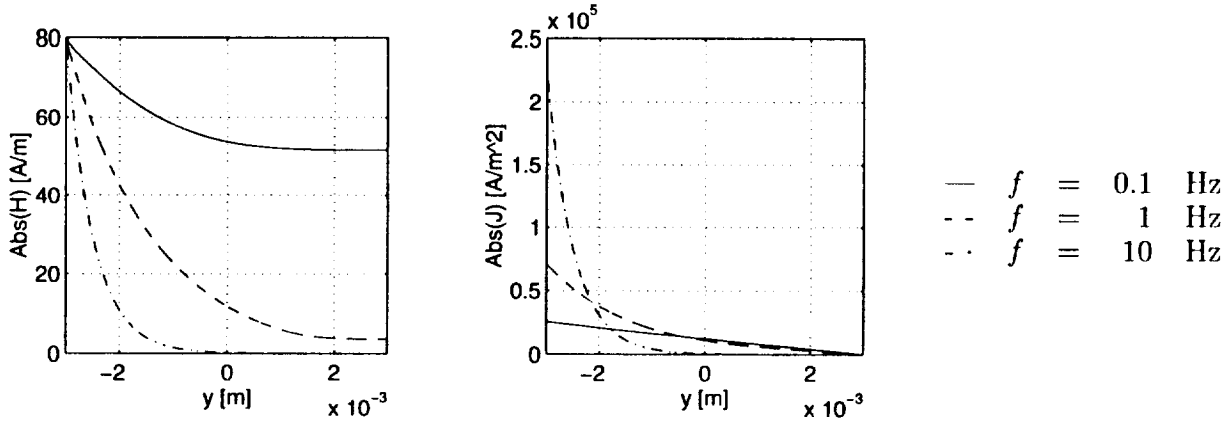

Figure 5: $|H_z(y)|$ and $|J_x(y)|$ for a cylinder without intersection

Figure 5 shows the decrease of the H-field near to the outer surface of the core and the increase of eddy currents near to the inner surface of the core with increasing frequency. The model parameters of the preceding section have been used.

[1]The unidirectional eddy current flow reminds us of a transformer with a shorted secondary winding. With the transformer equation, a model for eddy currents would be very simple. A transformer however has two windings and one core. Currents flow inside the windings and the core is only used as a magnetic material. An axial bearing has one winding and the core has two functions (for conducting and as a magnetic material). The transformer equation therefore would lead to an unacceptable error.

Comparison of the two boundary conditions

The generalized form of the flux equation can be written as:

$$\Phi = \Phi_0 \frac{\tanh(\gamma)}{\gamma} \tag{43}$$

with $\Phi_0 = A\mu H_0$ and with $\gamma = \alpha\frac{d}{2} \ldots \alpha d$.

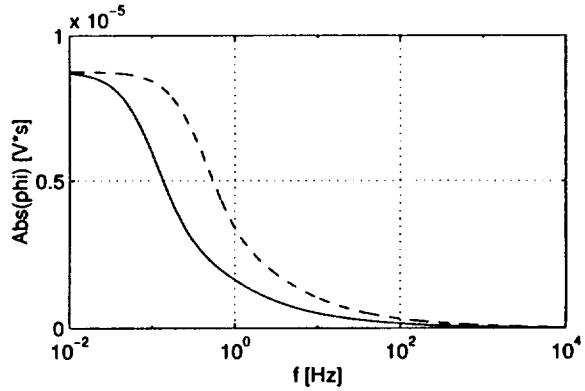

Figure 6: $|\Phi(f)|$ — cylinder without intersection
- - cylinder with intersection

A comparison of the flux equations (36) and (42) shows that γ is two times larger for unidirectional than for bidirectional eddy currents. Figure 6 shows the frequency dependent flux for both cases with the same Φ_0.
The flux bandwidth of bidirectional eddy currents is 4 times higher (see figure 6). This does not correspond to measurements which only show a factor of 2. This difference is caused by the frequency dependence of Φ_0.
In the case of bidirectional eddy currents, Φ_0 is constant for all frequencies. The H-field only changes inside the core and the boundary conditions at the surface of the core remain the same. This leads to frequency independance of the global H-field.
For unidirectional eddy currents the boundary conditions change at the surface of the core. This leads to a global change of the H-field and, therefore, to a change of Φ_0. In order to achieve analytical solutions it is necessary to expand the problem of modelling eddy currents with the problem of modelling inductances. Calculation of inductances can be done for simple geometric setups, but for complex geometries such as axial bearings analytical models are not available.
Several measurements have shown that the flux curves are similar for both eddy current cases. Therefore, the equations for bidirectional eddy currents can be used for unidirectional eddy currents too. It is clear that axial bearings with screw-holes or other gaps have uni- and bidirectional eddy currents and, therefore, the flux curve is between the two extreme eddy current cases.

The last boundary value H_0 can be found by closing the magnetic circuit. In order to build the complete magnetic circuit different materials have to be combined. Solutions for the flux are independent from the depth of the core (i.e. from the z-direction). Different materials lead to different solutions. It is clear that the flux changes in a transition region from one solution to the other. Finite Element analysis is used to calculate the flux distribution in a transition region between different materials. Figure 7 shows that the flux in the air gap is homogeneous even for high frequencies and that the transition region in the iron is small. Combining several materials is possible because the flux density distribution inside one material has little influence on the flux density distribution inside the next material.

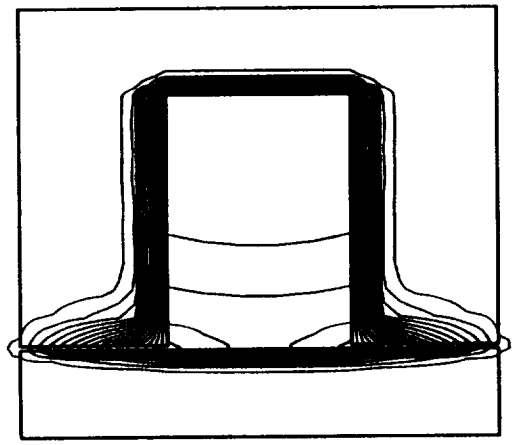

Figure 7: The flux inside the air gap is homogeneous even with a highly nonhomogeneous flux inside the unlaminated core ($f = 1\text{KHz}$).

For calculations with eddy currents, it is useful to define the cut-off frequency f_g of the flux decrease inside the core. In the literature f_g is called the cut-off frequency of the lamination (see also [Küp90]).

$$f_g = \frac{1}{\pi\sigma\mu d^2} \tag{44}$$

Axial bearing materials normally have either a very low f_g (unlaminated iron) or a very high f_g (laminated iron, special magnetic core materials such as Corovac[2] and air ($f_{g,air} \to \infty$)).

$$\oint H\mathrm{d}l = \sum_{m=1} H_m x_m = NI \tag{45}$$

$$\Phi = \int B_m \mathrm{d}A_m = A_m \mu_0 \mu_{r,m} H_m \frac{\tanh(\gamma_m)}{\gamma_m} \tag{46}$$

[2]Corovac is a high frequency core material with $\sigma \approx 5 \cdot 10^5 \text{S/m}$ and $\mu_r \approx 130$. The μ_r of Corovac is low compared to ferrite cores which are used for high frequency transformers. The machinability of Corovac is however much better.

Solving the system of equations (45) and (46) leads to the flux equation (for n different materials):

$$\Phi = \frac{\mu_0 N I}{\sum_{m=1}^{n} \frac{x_m}{\mu_{r,m} A_m} \frac{\gamma_m}{\tanh(\gamma_m)}} \tag{47}$$

The modelling of axial bearings cannot be improved using more than two terms of the sum. The first term represents all materials with low f_g and the second term includes all materials with a behaviour as air (f_g is very high and $\tanh(\gamma_m)/\gamma_m = 1$). This simplification is based upon the fact that a connection of two materials with similar f_g leads to:

$$a_1 \frac{\tanh(\gamma_1)}{\gamma_1} + a_2 \frac{\tanh(\gamma_2)}{\gamma_2} \approx a_3 \frac{\tanh(\gamma_3)}{\gamma_3} \tag{48}$$

The reduced flux equation is:

$$\Phi = \frac{\mu_0 N A I}{2x + \frac{l_{fe}}{\mu_r} \frac{\gamma}{\tanh(\gamma)}} = \mu_0 N A I \frac{1}{2x} \frac{1}{1 + \frac{1}{a_{fe}} \frac{\gamma}{\tanh(\gamma)}} \tag{49}$$

with:

$$a_{fe} = \mu_r \frac{2x}{l_{fe}} \tag{50}$$

All areas are normalized to the area of the air gap A. x is the length of the air gap (including lengths of materials with very high f_g) and l_{fe} is the length of the unlaminated core.

Saturation

In the previous calculations μ_r has been assumed to be constant. Saturation of the magnetic material leads to a limit value for the flux. The solution for the flux therefore gives unrealistically high values at the surface. Even with simple models for saturation (e.g. Fröhlich model [Sto74]), it is not possible to derive an analytical solution for the differential equations. Numerical calculations have shown that the behaviour of the H-field with saturation is very similar to the behaviour without saturation. It is therefore not necessary to include saturation into a model for eddy currents.

Equivalent Electrical Circuit

When x is assumed to be constant, the impedance of an eddy current affected coil can be written as:

$$Z = \frac{U}{I} = \frac{N \frac{\mathrm{d}\Phi}{\mathrm{d}t}}{I} = j\omega L_0 \frac{1}{1 + \frac{1}{a_{fe}} \frac{\gamma}{\tanh(\gamma)}} \tag{51}$$

with:

$$L_0 = \mu_0 N^2 A \frac{1}{2x} \tag{52}$$

Forces

The magnetic force is proportional to the square of the flux. Therefore a reduction of the flux due to eddy currents will also reduce the force to:

$$F = \frac{\Phi^2}{\mu_0 A} = \frac{K}{4}\frac{I^2}{x^2}\frac{1}{\left(1 + \frac{1}{a_{fe}}\frac{\gamma}{tanh(\gamma)}\right)^2} \tag{53}$$

with:

$$K = \mu_0 N^2 A \tag{54}$$

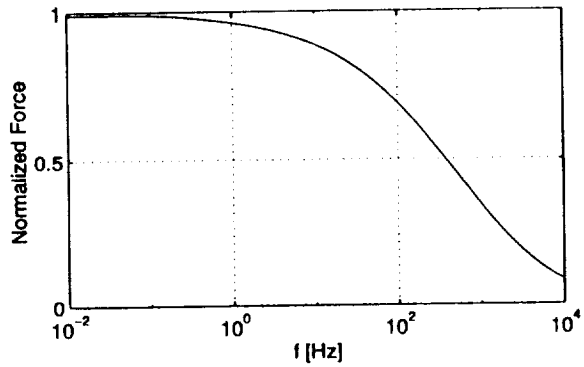

Figure 8: Normalized force dynamics $|F/F_{DC}|$ of an axial bearing ($f_g \approx 0.02$Hz, $a_{fe} \approx 200$)

NONLINEAR PARAMETER IDENTIFICATION

Parameter Identification

It is clear that the impedance of a coil not only depends on the inductance affected by the eddy currents. An impedance model must also include the coil resistance R_{cu}, the coil inductance L_{cu} and the coil capacitance C_{cu} (see figure 9). The last two parameters are necessary to model the frequency range above 10kHz. Thus, the total impedance is:

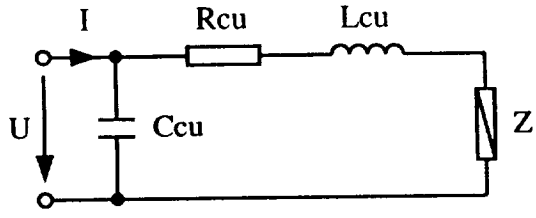

Figure 9: Complete equivalent electrical circuit

$$Z_{tot} = \frac{1}{j\omega C_{cu}} || (Z + R_{cu} + j\omega L_{cu}) \tag{55}$$

Robustness of the identification can be improved by defining the constraints. The authors used the constraint algorithm from the MATLAB Optimization Toolbox. The parameter range described below is sufficient to approximate all measured axial bearings. Less stringent constraints are possible, but computational time increases.
All parameter ranges excluding R_{cu} are written with exponential notation. The fitting algorithm therefore fits the exponent of the parameters. This method avoids the value 0 and guarantees convergence.

The ranges of the fitted parameters are given below.

$$\begin{array}{lllll} R_{cu} & = 0 & \ldots & 2 & \Omega \\ C_{cu} & = 1 \cdot 10^{-12} & \ldots 1 \cdot 10^{-9} & & F \\ L_{cu} & = 1 \cdot 10^{-6} & \ldots 1 \cdot 10^{-3} & & H \\ L_0 & = 1 \cdot 10^{-3} & \ldots 1 \cdot 10^{0} & & H \\ a_{fe} & = 1 \cdot 10^{0} & \ldots 1 \cdot 10^{3} & & \\ f_g & = 1 \cdot 10^{-3} & \ldots 1 \cdot 10^{1} & & Hz \end{array}$$

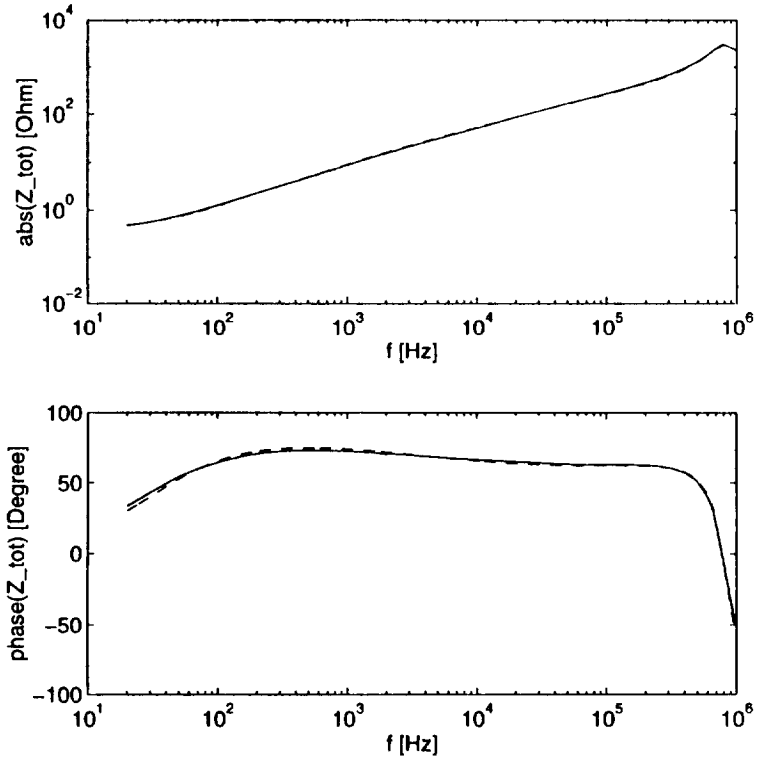

Figure 10: Example 1: Axial bearing with unlaminated core and target.
— : calculated data, - - : measured data
Identified parameters: $R_{cu} \approx 1.5\Omega, C_{cu} \approx 800pF, L_{cu} \approx 120\mu H, L_0 \approx 12mH, a_{fe} \approx 3, f_g \approx 7Hz$

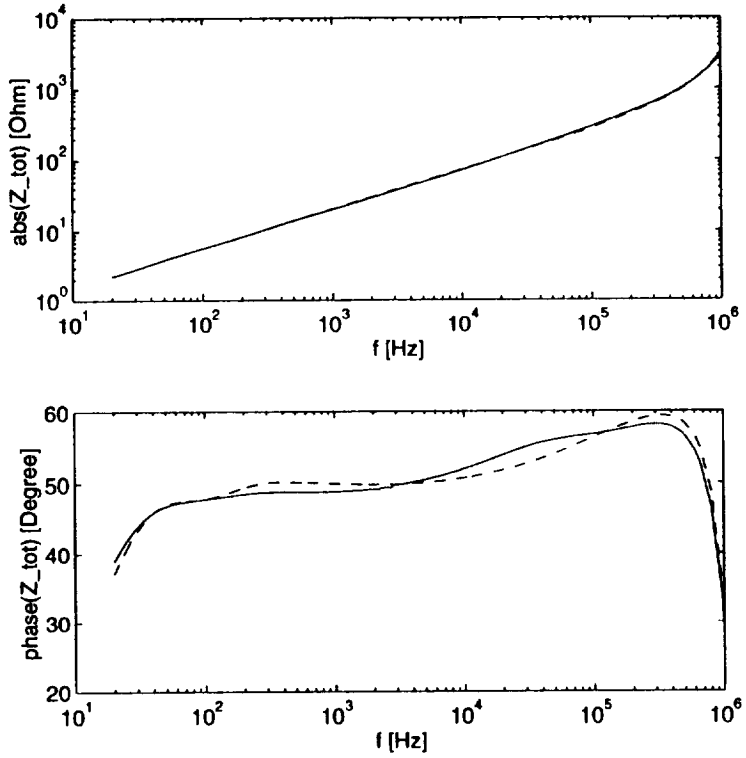

Figure 11: Example 2: Axial bearing with a Corovac core and an unlaminated target.
— : calculated data, - - : measured data
Identified parameters: $R_{cu} \approx 0.4\Omega, C_{cu} \approx 150pF, L_{cu} \approx 120\mu H, L_0 \approx 1.4mH, a_{fe} \approx 150, f_g \approx 0.12Hz$

The fitting error e is approximately 5% with the usual air gap and increases up to 10% when the air gap is small and the flux is saturated and is given by:

$$e = \sqrt{\frac{1}{n}\sum^{n}\left|1 - \frac{Z_{fit}}{Z_{meas}}\right|^2} \tag{56}$$

where n is the number of measured values, Z_{fit} the fitted impedance and Z_{meas} the measured impedance.

Losses

The spectral losses of an axial bearing are given by:

$$P = \text{real}(U\text{conj}(I)) = |U|^2\text{real}(\text{conj}\left(\frac{1}{Z_{tot}}\right)) \tag{57}$$

Figure 12 shows normalized loss based on impedance measurements of an axial bearing with a Corovac core. At low frequencies losses are very high due to R_{cu}. With increasing frequency

losses decrease. It is therefore useful to choose the switching frequency of an amplifier as high as possible. As mentioned in section *Comparison of the two boundary conditions*, a radial intersection of an axial bearing can increase the bandwidth of the flux and leads to lower losses. It is only sufficient to intersect unlaminated parts of the core with low f_g, i.e. in most cases the axial bearing target. An axial bearing without intersection suffers more than 40% higher loss than one with intersection at frequencies typically used for switching amplifiers (20 - 200 kHz).

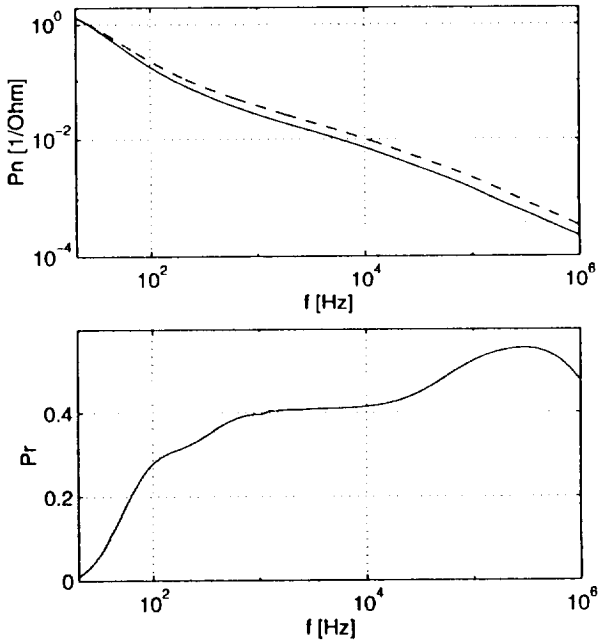

Figure 12: upper plot: normalized losses $P_n = P/|u|^2$ of an axial bearing with Corovac core and steel target (— P_1: target intersected , - - P_2: target not intersected)
lower plot: relative difference between the two curves of the upper plot $P_r = (P_2 - P_1)/P_1$

Measurement

Measurements of axial bearing impedances are made with a LCR-meter (HP 4284A) including a power current source (HP 42841A). The LCR-meter has the possibility to measure with logarithmically sweeped frequencies from 20Hz up to 1MHz. A host computer controls the measurement via GPIB-interface.
The power current source allows measurements of very high inductances and can superpose the measurement signal with a DC-bias current of up to 20A.

CONCLUSIONS

A model for eddy currents in axial bearings has been derived which can describe the behaviour for a wide frequency range. From the analytical solution for the flux, the impedance, the magnetic force and the losses can be calculated. Measurements have shown that the model is very precise.

REFERENCES

[AS65] Milton Abramowitz and Irene A. Stegun. *Handbook of Mathematical Functions.* Dover Publications, Inc., New York, 1965.

[Gro78] Emil Grosswald. *Bessel Polynomials.* Springer-Verlag, Berlin, 1978.

[Haf87] Christian Hafner. *Numerische Berechnung elektromagnetischer Felder.* Springer-Verlag, Berlin, 1987.

[Hec75] Carl Heck. *Magnetische Werkstoffe und ihre technischen Anwendungen.* Hüthig, Heidelberg, 1975.

[Ins94] Institut für Elektrische Maschinen, ETH Eidgenössische Technische Hochschule, Zürich. *FEMAG Benutzeranleitung*, 1994.

[Jac83] John D. Jackson. *Klassische Elektrodynamik.* de Gruyter, Berlin, 1983.

[Küp90] Karl Küpfmüller. *Einführung in die theoretische Elektrotechnik.* Springer-Verlag, Berlin, 1990.

[KXMH92] J. Knight, Z. Xia, E. McCaul, and H. Hacker. Determination of Forces in a Magnetic Bearing Actuator: Numerical Computation With Comparison to Experiment. *Journal of Tribology*, 114, 1992.

[LD89] Dimitris Labridis and Petros Dokopoulos. Calculation of Eddy Current Losses in Nonlinear Ferromagnetic Materials. *IEEE Transactions on Magnetics*, 25, May 1989.

[May91] I.D. Mayergoyz. *Mathematical Models of Hysteresis.* Springer-Verlag, New York, 1991.

[MH94] T. Mizuno and T. Higuchi. Experimental Measurement of Rotational Losses in Magnetic Bearings. In *Fourth International Symposium on Magnetic Bearings*, Zurich, 1994.

[Sto74] Richard Stoll. *The analysis of eddy currents.* Clarendon Press, Oxford, 1974.

[TK85] J.A. Tegopoulos and E.E. Kriezis. *Eddy Currents in Linear Conducting Media.* Elsevier, Amsterdam, 1985.

[Tra86] Alfons Traxler. *Eigenschaften und Auslegung von berührungsfreien elektromagnetischen Lagern.* PhD thesis, ETH Eidgenössische Technische Hochschule, Zürich, 1986.

Session 12 -- Precision Applications

Chairman: Karl Boden
KFA-IGV/Hideo Sawada, NAL